
This is an electronic reprint of the original article.
This reprint may differ from the original in pagination and typographic detail.

Adamczyk, Zbigniew; Morga, Maria; Kosior, Dominik; Batys, Piotr
Conformations of Poly- L -lysine Molecules in Electrolyte Solutions

Published in:
Journal of Physical Chemistry C

DOI:
[10.1021/acs.jpcc.8b07606](https://doi.org/10.1021/acs.jpcc.8b07606)

Published: 11/10/2018

Document Version
Peer-reviewed accepted author manuscript, also known as Final accepted manuscript or Post-print

Published under the following license:
Unspecified

Please cite the original version:
Adamczyk, Z., Morga, M., Kosior, D., & Batys, P. (2018). Conformations of Poly- L -lysine Molecules in Electrolyte Solutions: Modeling and Experimental Measurements. *Journal of Physical Chemistry C*, 122(40), 23180-23190. <https://doi.org/10.1021/acs.jpcc.8b07606>

This material is protected by copyright and other intellectual property rights, and duplication or sale of all or part of any of the repository collections is not permitted, except that material may be duplicated by you for your research use or educational purposes in electronic or print form. You must obtain permission for any other use. Electronic or print copies may not be offered, whether for sale or otherwise to anyone who is not an authorised user.

Conformations of Poly-L-lysine Molecules in Electrolyte Solutions: Modeling and Experimental Measurements

Zbigniew Adamczyk,[§] Maria Morga,^{,§} Dominik Kosior,[§] and Piotr Batys,^{§,‡,*}*

[§]Jerzy Haber Institute of Catalysis and Surface Chemistry, Polish Academy of Sciences,
Niezapominajek 8, 30–239 Krakow, Poland.

[‡]Department of Chemistry and Materials Science, Aalto University, P.O. Box 16100, 00076
Aalto, Finland

^{*}Department of Bioproducts and Biosystems, Aalto University, P.O. Box 16100, 00076 Aalto,
Finland

ABSTRACT

Physicochemical properties of poly-L-lysine (PLL) hydrobromide were determined by Molecular Dynamics (MD) modeling and a variety of experimental techniques. Primarily, the density, the chain diameter, the monomer length and PLL molecule conformations were theoretically calculated. These results were applied for the interpretation of experimental data acquired for

PLL sample of the average molar mass equal to 122 kg/mol. They comprised the diffusion coefficient, the hydrodynamic diameter and the electrophoretic mobility of molecules determined for ionic strength range 2×10^{-5} to 0.15 M and pH 5.6. Using these data, the electrokinetic charge and the effective ionization degree of PLL molecules were determined as a function of ionic strength. Additionally, precise dynamic viscosity measurements for dilute PLL solutions were performed yielding the intrinsic viscosity, which decreased from 2420 to 120, for ionic strength of 2×10^{-5} and 0.15 M, respectively. This confirmed that PLL molecules assume extended conformations in accordance with theoretical modeling. These data enabled to determine the molecule length, the chain diameter and its effective molecule cross-section area for various ionic strengths. Therefore, it was concluded that the combined dynamic light scattering and viscosity measurements supplemented by MD modeling furnish reliable information about PLL macromolecule conformations in electrolyte solution. Beside significance for basic science, the results obtained in this work can be exploited for precisely determining molar mass of macroions.

1. Introduction

Extensive range of macroion (polyelectrolyte) applications is based on the efficient adsorption of the macromolecules at various surfaces, which is then exploited for various applications, like for example preparing anti-fouling coatings preventing bacteria adhesion.¹⁻³ In other processes, macroion adsorption is applied to produce adhesive substrates for protein and enzyme immobilization, separation,⁴ and bio-sensing.⁵ Another application is due to consecutive adsorption of cationic and anionic macroions, according to layer by layer (LbL) process, which is widely adapted in nanocapsule formulations, used for controlled drug delivery.^{6,7}

Among various macroions, poly-L-lysine (PLL) whose molecule is solely composed of naturally occurring lysine amino acids residues, has acquired considerable attention. This is mainly caused by a stable and positive charge of PLL molecules in aqueous solutions, which occurs over a wide range of pH up to 11.^{8,9} Therefore, PLL is used in variety of industrial and scientific branches for medical applications, e.g., as a model drug,¹⁰⁻¹² for microencapsulation of islets^{13,14} and cells,¹⁵⁻¹⁷ chromosomal preparations,¹⁸ biomimetic mineralization,¹⁹⁻²¹ cell attachment,²² biosensors and biosensor arrays.⁸

Because of the wide range of applications, extensive research has been conducted in order to investigate PLL structure,²³⁻²⁵ surface properties,^{26,27} and adsorption at various substrates.^{26,28-30}

Barrantes et al.³¹ investigated the formation of PLL/HEP (heparine) multilayers adsorbed at various pHs on silica and gold wafers. The mass of multilayers was measured using QCM-D (quartz crystal microbalance with dissipation) and ellipsometry. Moreover, from the viscoelastic properties it was concluded that at acidic conditions a side-on conformation of PLL molecules occurred whereas at pH 7 and 8.5, the molecules adopted α -helical conformation. In another work, Barrantes et al.³² studied the influence of PLL/HEP multilayers (films) on the adsorption of bovine serum albumin (BSA), immunoglobulin (IgG) and fibrinogen. The experiments were carried out in phosphate buffered saline ($I = 0.148$ M and pH 7.4). The adsorption of macroions and proteins was studied using ellipsometry, QCM-D and AFM (atomic force microscopy). It was shown that the protein adsorption only occurred at PLL terminated multilayers.

Porus et al.^{33,34} studied sodium poly(styrene sulfonate) (PSS), PAH poly(allylamine hydrochloride) (PAH) and PLL adsorption at silica substrate using optical reflectometry and quartz crystal microbalance (QCM). Both the dry and wet mass were determined that allowed to

calculate the hydration degree of PLL molecules. It was also shown that the thickness of PLL layers varied between 1.3 and 1.4 nm for pH 4 and 10 respectively.

Choi et al.³⁵ studied the formation of PLL monolayers on various substrates, such as the carboxyl functionalized, amine-functionalized and bare silica using the QCM-D method. The adsorption was carried out from PLL solutions characterized by large concentration of 2000 mg L⁻¹ at pH range 2 to 12. The Voigt-based viscoelastic analysis was performed assuming the PLL film density equal to 10³ kg m⁻³ and the viscosity of bulk solution equal to 0.001 Pa s⁻¹, respectively.

Craig et al.³⁶ investigated the formation of PLL/PGA (polyglutamic acid) films applying the layer-by-layer self-assembly technique using ellipsometry and QCM-D.³⁷ The films were deposited on thiol-modified gold surface.

Richert et al.²⁹ investigated interactions of chondrosarcoma cells with PLL/(poly-L-glutamic acid) (PGA) multilayers in a serum-containing medium for various pHs using the optical waveguide lightmode spectroscopy (OWLS), QCM-D, streaming potential measurements and AFM.

Picart et al.²⁶ studied the deposition of PLL/hyaluronic acid (HA) multilayers at gold holders and glass slides in order to prepare a new kind of biocompatible film. The investigation was carried on using optical waveguide lightmode spectroscopy, streaming potential measurements, atomic force microscopy (AFM) and QCM-D.

Ren et al.³⁸ used the layer-by-layer self-assembly method in order in order to produce PLL and deoxyribonucleic acid (DNA) enzymatic biodegradable films deposited on quartz substrates. The process of film formation was monitored by UV–vis spectrometry, and atomic force microscopy.

Shan et al.³⁹ investigated functionalization of graphene sheets by PLL using UV-vis spectroscopy, Fourier transform infrared spectroscopy (FTIR), AFM, energy dispersive X-ray spectroscopy (EDX), and cyclic voltammetry (CV). It was assumed that graphene sheets play an important role as connectors to assemble active amino groups of PLL, which provide an efficient platform for the attachment of bioactive molecules.

However, despite of this extensive experimental effort, the fundamental physicochemical properties of PLL molecules in aqueous solutions, especially their molecular density, size, shape, and conformation under various ionic strengths, especially in diluted aquatic solutions, remain largely unknown. The lack of this data prohibits a proper interpretation of experimental results concerning PLL adsorption at various substrates and multilayer formation efficiency.

Given the deficit of reliable experimental data, the goal of this work is to perform thorough characteristics of PLL molecules in aqueous solutions for a broad range of ionic strength using a variety of complementary experimental methods based on electrophoresis, dynamic light scattering (DLS) and viscosity measurements, which is also a novel approach for determining basic physicochemical parameters for other elongated polyelectrolyte molecules. The diffusion coefficient, the hydrodynamic diameter, the effective (electrokinetic) charge per molecule, and the intrinsic viscosity are determined. The experimental data are quantitatively interpreted in terms of the all-atom Molecular Dynamic (MD) modeling. In this way, valid clues about the PLL molecule conformations are acquired, especially the molecule chain diameter, the extended length and the effective cross-section area are determined for the first time. This has significant implication for predicting adsorption mechanisms and controlling adsorption process of PLL molecules at solid/electrolyte interfaces and for a quantitative interpretation of experimental data derived from the streaming potential measurements,^{40,41} quartz microbalance,^{33,34} and other

experimental techniques that require proper calibration. Moreover, the results obtained in this work allow also for elaboration of a procedure for determining molar mass of polypeptide macroions, in a more precise way than with applying conventional methods.

2. Experimental section

2.1. Materials

Poly-L-Lysine hydrobromide, a synthetic polypeptide having a molar mass of 150–300 kg mol⁻¹ (determined by viscosity) and 75–189 kg mol⁻¹ (determined by MALLS), hereafter referred to as PLL, was purchased from Sigma Aldrich Merck KGaA, Darmstadt, Germany.

The stock and dilute solutions of PLL were prepared by dissolving a proper amount of solid PLL in NaCl. The NaCl solutions of a precisely known concentration were prepared using deionized water obtained using Milli-Q Elix & Simplicity 185 purification system from Millipore SAS Molsheim, France and analytical grade NaCl purchased from Sigma Aldrich Merck KGaA, Darmstadt, Germany.

2.2. Methods

The electrophoretic mobility and diffusion coefficients of PLL molecules under various conditions were determined by the electrophoretic measurements (Laser Doppler Velocimetry (LDV) technique) and the dynamic light scattering (DLS) using the Malvern Zetasizer Nano ZS apparatus.

The density of PLL solutions for various ionic strengths was determined using the high precision Anton Paar DMA 5000 M densitometer.

The kinematic viscosity of PLL solutions of defined mass concentrations was measured using certified Cannon-Ubbelohde semi-micro dilution viscometer, which requires small volumes of polypeptide solution (up to 5 ml) and permits easy serial dilutions. The whole set-up was equipped with a thermostat that allowed a precise control of temperature during the measurement. Knowing the kinematic viscosity and density of PLL solution enabled to calculate the dynamic viscosity. The measurements were carried out for the range of PLL concentration of 50–500 mg L⁻¹ at a fixed NaCl concentration (ionic strengths), where the relative viscosity η_r was smaller than 1.3. A typical error of intrinsic viscosity determination was equal to 0.2–1% for NaCl concentration equal to 0.15 and 2×10^{-5} M, respectively.

All measurements were performed at 298 K and pH of 5.4–5.6.

2.3. Theoretical Calculations

The Gromacs 5.1.4 package^{42,43} was used for all-atom molecular dynamics (MD) modeling of the PLL molecules of various molar mass with the Amber 03 force field.⁴⁴ For water, in compliance with the force-field choice, the explicit TIP3P model was employed.⁴⁵ The PLL molecules, generated using Avogadro software,⁴⁶ were solvated by water molecules in a cubic box with the size equal to 10–22 nm depending on PLL molar mass. The counter-ions were introduced by a random replacement of water molecules in order to obtain neutral systems characterized by ionic strength equal to 10^{-3} M.

Energy minimization was performed to relax the initial structure. Then, a 150 ns NPT ensemble simulation run was performed. The first 50 ns were considered as equilibration and omitted in the data analysis. The V-rescale thermostat⁴⁷ with coupling constant 0.1 ps was applied at reference temperature $T = 298$ K. The PLL was coupled to the heat bath as one thermostating group while water and the ions were coupled as another group. The pressure was

controlled by the isotropic Parrinello-Rahman barostat⁴⁸ with 2 ps coupling constant and reference pressure 1 bar. To calculate long-range electrostatic interactions, the PME method was used.⁴⁹ The van der Waals and short-range repulsive interactions were described using the Lennard-Jones potential with a 1.0 nm cut-off. Throughout the simulations, all the bonds in the PEs and water molecules were controlled by the LINCS⁵⁰ and SETTLE⁵¹ algorithms, respectively. A 2 fs time step within the leap-frog integration scheme was applied and the trajectories were written every 10 ps. Periodic boundary conditions were applied in all directions. All simulation visualizations presented are done using the VMD software package.⁵² For each frame, the PLL end-to-end distance was calculated as the distance between the terminal atoms of the polyelectrolyte backbone, using *gmx polystat* GROMACS software package. The average distance between the C_α atoms as a function of time was calculated using *gmx distance* tool from GROMACS.

3. Results and Discussion

3.1. Theoretical modeling results

The calculations presented hereafter were performed for PLL molecules composed of 25, 50 and 75 monomers (repeat units). The primary goal of these calculations was to determine the density of the molecule in aqueous solutions, the chain diameter and the maximum extended (contour) length of the molecule. Extrapolation of these results to larger molar mass of PLL furnishes theoretical data that are inaccessible for direct theoretical modeling because of excessive time of computations. In order to assess the validity of this extrapolation, through experimental studies were performed yielding the diffusion coefficient, hydrodynamic diameter, ionization degree, and intrinsic viscosity. These parameters can be directly related to the PLL

molecule density, chain diameter, and extended length derived from modeling. Typical snapshot of PLL chain conformations obtained for ionic strength of 10^{-3} M and various monomer numbers are shown in Figure 1.

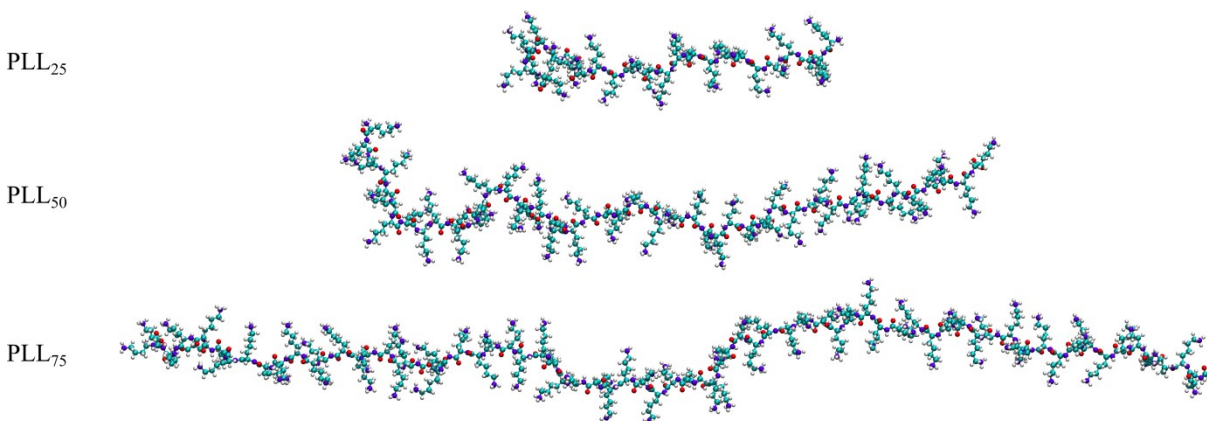


Figure 1. Snap–shots of PLL chain conformations of various monomer numbers derived from MD modeling for 10^{-3} M ionic strength.

The MD modeling was used to determine the PLL molecule density via the dilution method. Accordingly, the size of the simulation boxes, where a single PLL molecule was confined, was systematically decreased that resulted in the increase in the mass fraction from 0 to 0.01 (see Figure 2).

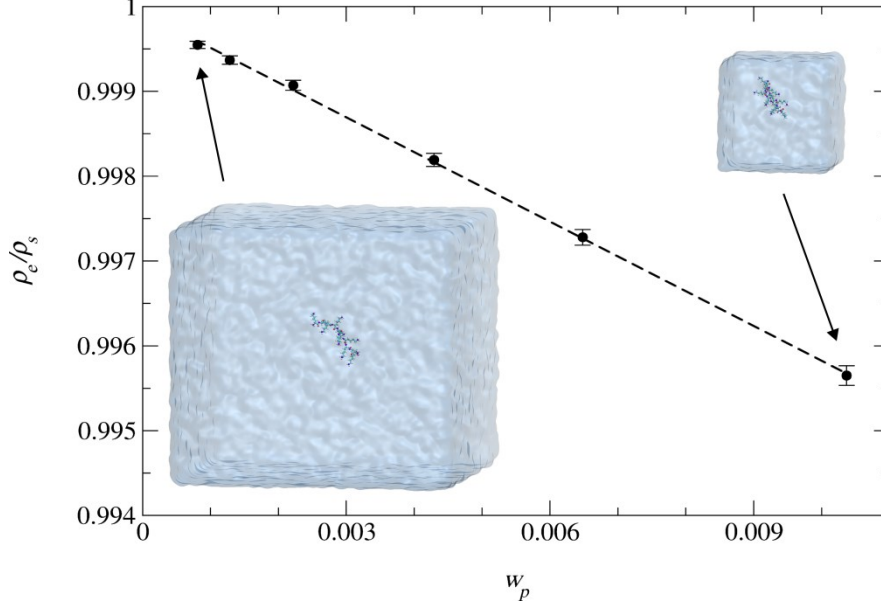


Figure 2. The dependence of ρ_e/ρ_s on the mass fraction w_p determined via MD modeling. The dashed line shows the linear fitting of theoretical results. The corresponding simulation boxes for the lowest and highest w_p are shown as insets.

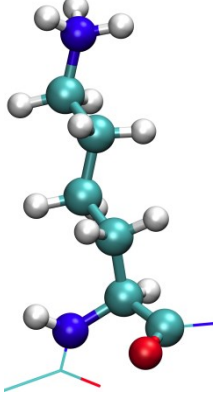
The density of these systems ρ_s as well as the pure solvent ρ_e was determined in these runs. Then, the dependence of ρ_e/ρ_s on w_p was plotted (see Figure 2) and fitted by a straight line characterized by the slope s_p and the density was calculated from the formula:

$$\rho_p = \frac{\rho_e}{1 + s_p} \quad (1)$$

In this way, one obtains at temperature of 298 K, $\rho_p = 1.60 \pm 0.02 \times 10^3 \text{ kg m}^{-3}$.

For the sake of convenience, the theoretical data obtained from modeling are collected in Table 1.

Table 1. Physicochemical characteristics of PLL derived from MD modeling, $T = 298$ K.

Quantity (unit), symbol	Value	Remarks
Chemical structure of monomer		Monomer molar mass, $M_I = 0.209 \text{ kg mol}^{-1}$
Density (kg m^{-3}), ρ_p	$1.60 \pm 0.02 \times 10^3$	This work, MD modeling
Specific volume of molecule (nm^3/kg), v_s	1.04 ± 0.01	Calculated as $1024/(\rho_p A_v)$
Monomer volume (nm^3), v_p	0.217 ± 0.002	Calculated as $10^{-3} \times v_s M_I$
Monomer length for the extended chain, l_m (nm)	0.330 ± 0.004	This work, MD modeling

It should be mentioned that in every MD run, the conformation of PLL molecule dynamically changed in time. In order to quantify this effect, histograms presenting the fluctuations in the end-to-end length of the molecule are constructed for various PLL molar mass. In Figure 3 histograms obtained for PLL chains containing 25, 50, and 75 monomers and NaCl concentration of 10^{-3} M are shown. From such histograms the average end-to-end length of PLL the molecule was determined (Table 1). The obtained histograms are relatively smooth, which suggests that the conformational sampling was representative enough and that the timescale applied in this work was sufficient. As seen in Figure 3, the average end-to-end length was a linear function of the number of monomers N_m :

$$L_e = l_a N_m \quad (2)$$

where l_a is the constant equal to 0.220 ± 0.003 . One should expect that this is a valid estimate of the monomer length in the limit of low ionic strength. Therefore, knowing l_m one can predict by extrapolation the average length of the PLL molecule of larger molar mass than it is feasible in MD modeling.

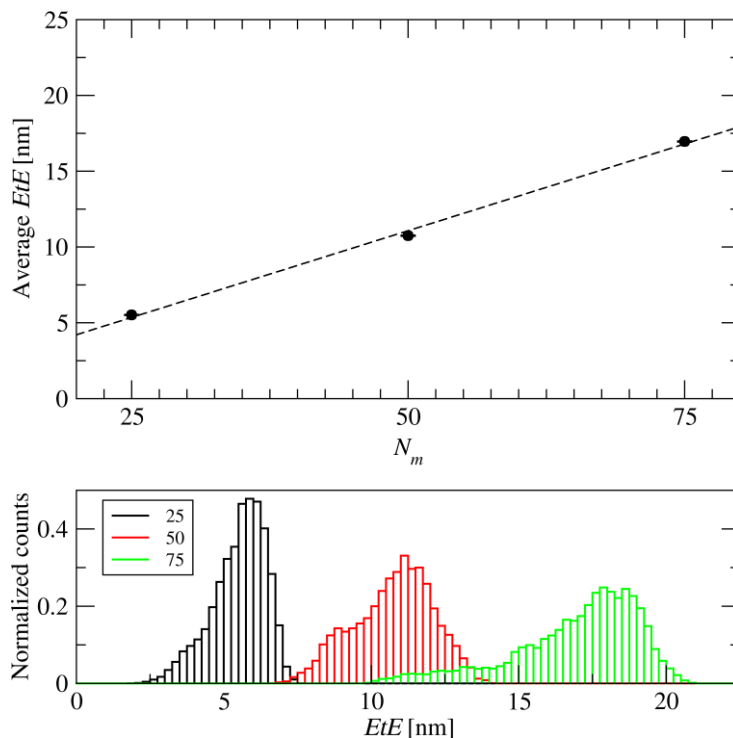


Figure 3. Upper part: the average PLL end-to-end (EtE) length as a function of the number of monomers. The line denotes linear fitting of theoretical data. Lower part: the end-to-end distance distribution for the PLL molecules with different number of repeat units derived from MD modeling (NaCl concentration equal to 10^{-3} M).

On the other hand, the volume of a single monomer, $v_p = 0.217 \pm 0.002$ nm³ was calculated using the PLL density and its molar mass (see Table 1). Analogously, for each of the molecules considered in the modeling, its volume was calculated (Table 2). Using these parameters and considering the average end-to-end length obtained from simulation the effective chain diameter

of the molecule was calculated assuming its cylindrical shape using the equation $d_c = (v_m / (\pi L_e))^{1/2}$. For all chain lengths the diameter was equal to 1.12 nm for ionic strength of 10^{-3} M.

Table 2. Properties of the PLL chains with 25, 50, and 75 repeat units obtained from MD modeling.

Quantity (unit), symbol	Number of monomers, N_m		
	25	50	75
Average end-to-end distance (nm), L_e	5.52 ± 0.01	10.74 ± 0.02	16.96 ± 0.02
Maximum end-to-end distance (nm) (contour length)	8.25 ± 0.02	16.5 ± 0.02	24.8 ± 0.02
Molecule volume (nm ³), v_m	5.43 ± 0.05	10.85 ± 0.10	16.28 ± 0.15
Chain diameter (nm), d_c ($I = 10^{-3}$ M)	1.12 ± 0.01	1.13 ± 0.01	1.11 ± 0.01
Diameter of extended chain (nm) ($I = 0$ M)	0.92 ± 0.01	0.92 ± 0.01	0.92 ± 0.01

Because the counter-ions were added to the system, in order to keep the overall charge neutral, in the MD modeling one was unable to gain a direct access to the physicochemical properties of the molecule in the limit of low ionic strength. However, using the PLL conformation at $I = 10^{-3}$ M, the PLL contour length and the diameter of extended chain were determined applying the concept of a freely jointed chain (Kuhn chain).^{53,54} Accordingly, the PLL molecule was considered as a collection of $N_m/2$ segments as presented in Figure 4. To preserve the trans conformation of the PLL, the length of a single segment b was set to be equal to the average distance between every other C_α atom, averaged over the simulation time. The distance $b/2$ can be therefore considered as the single monomer length for the extended chain in trans conformation, and denoted hereafter as l_m (see Table 1). This enabled to calculate the contour

length as a product of the single monomer length and the number of monomers, i.e., $N_m b/2$, where $b = 0.660 \pm 0.004$ nm. Then, using the volume of the molecule and its contour length, the diameter of extended chain was calculated (see Table 2).

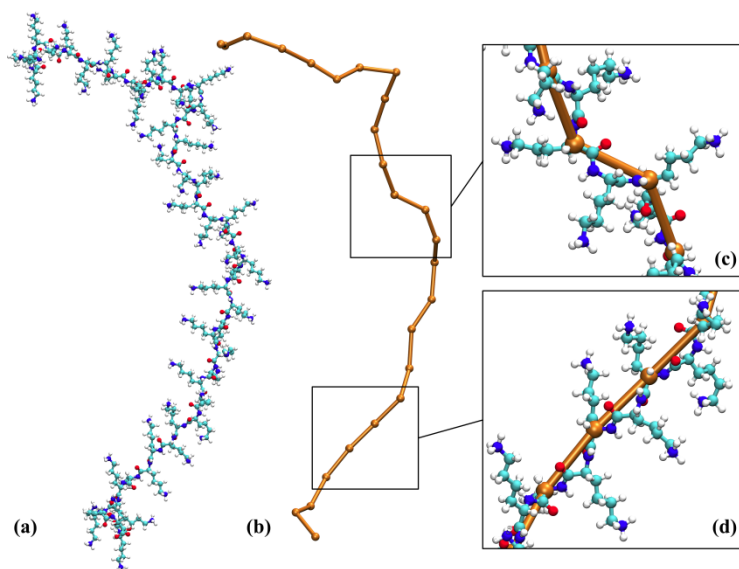


Figure 4. (a) The exemplary conformation of the PLL₅₀ and (b) the same conformation divided into 25 segments. The zoom of the (c) curved and (d) straight chain fragment. The odd C_α atoms are marked as orange spheres.

3.2. Basic physicochemical characteristics of PLL molecules

The density of PLL molecules, which up to our knowledge has not been reported so far in the literature, was determined by the solution dilution method previously applied in Ref. ⁵⁵. Briefly, the PLL solutions in NaCl (concentration range 2×10^{-5} –0.15 M) of known mass fraction w_p varied within the range 0 – 5×10^{-4} are prepared. The density of these solutions ρ_s is measured using the densitometer with a precision of 5×10^{-3} kg m⁻³. The dependence of ρ_e/ρ_s on w_p obtained in this way (where ρ_e is the density of the pure NaCl solution) is fitted by a straight line having

the slope s_p (see Figure 5). Then, the PLL molecule density in the NaCl solutions (ρ_p) is calculated from eq 1.

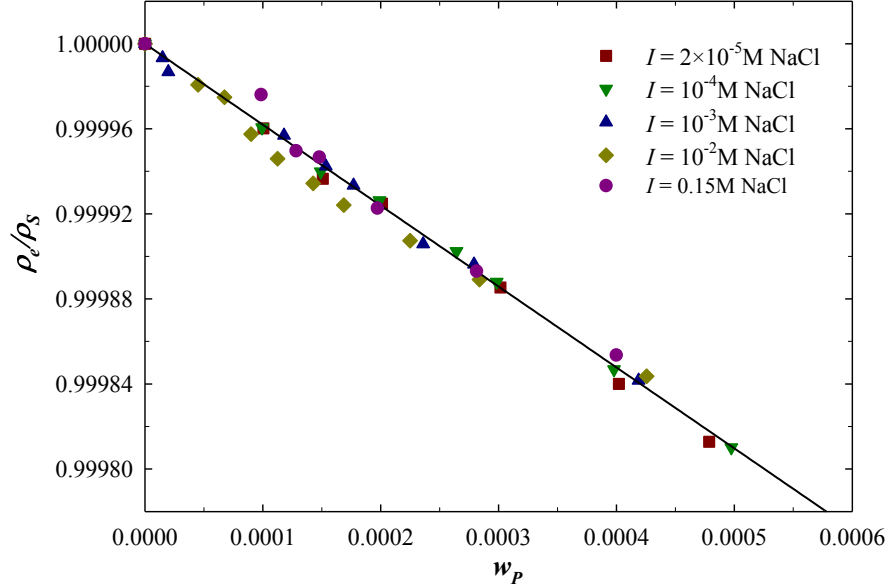


Figure 5. The dependence of the ρ_e/ρ_s on the mass fraction of PLL solutions w_p for $I = 2 \times 10^{-5}$ to 0.15 M, pH 5.4–5.6. The solid line shows the linear fit ($y = ax + b$) of experimental data with the slope s_p equal to -0.38.

It was calculated in this way that at the temperature of 298 K, $\rho_p = 1.61 \pm 0.01 \text{ g cm}^{-3}$ for the NaCl concentration range 2×10^{-5} to 0.15 M that agrees with the value derived from MD modeling. Knowing the PLL density and using the average molar mass of $1.22 \times 10^2 \text{ kg mol}^{-1}$ (Table 3) one can calculate that the volume of one molecule v_m equals to 126 nm^3 . Moreover, considering that the molar mass of the monomer is equal to $0.209 \text{ kg mol}^{-1}$, there is on average $N_m = 584$ monomers in the PLL molecule used in the experimental studies. Additionally, using the chain diameter (0.92 nm) derived from MD modeling one can calculate the maximum extended length of the molecule, assuming its cylindrical shape, from the formula $L_e = 4v_p/(\pi d_c^2)$. It is equal to 190 nm that corresponds to the aspect ratio parameter $\lambda = L_e/d_c$ of 206 (see Table 3).

Table 3. Physicochemical characteristics of PLL used in experimental studies, $T = 298$ K, pH 5.4–5.6.

Quantity (unit), symbol	Value	Remarks
Molar mass (kg mol ⁻¹), M	$1.5 \times 10^2 - 3 \times 10^2$	Manufacturer, viscosity method
Molar mass (kg mol ⁻¹), M	$7.5 \times 10^1 - 1.9 \times 10^2$	Manufacturer, MALLS
Average molar mass, (kg mol ⁻¹), \overline{M}_n	1.22×10^2	Manufacturer, number averaged, MALLS
Density (kg m ⁻³), ρ_p	$1.61 \pm 0.01 \times 10^3$	This work, dilution method
Average molecule volume (nm ³), v_p	126	Calculated as $10^{27} \times \overline{M}_n / (\rho_p A v)$
Equivalent sphere diameter (nm)	6.22	Calculated as: $(6 v_p / \pi)^{1/3}$
Average number of monomers, \overline{N}_m	584	Calculated as \overline{M}_n / M_1
Average extended length (maximum) (nm), \overline{L}_e	190	Predicted from the cylinder (rod) model: $4 v_p / (\pi d_c^2)$
	192	Calculated as: $\overline{N}_m l_m$ Using the MD l_m value
Average aspect ratio parameter, λ	206	Calculated from the cylinder (rod) model, \overline{L}_e / d_c
	209	Predicted from MD calculations

One can also predict that for a full ionization there should be 584 elementary charges per one PLL molecule. This would produce the net charge per one molecule equal to 9.34×10^{-17} C. However, this large nominal charge is significantly compensated in electrolyte solutions as a result of the specific adsorption of counter-ions often referred to as Manning's ion condensation.

The significance of this effect was quantitatively evaluated in a recent publication⁵⁶. Experimentally, the effective molecule charge in solutions can be estimated via the electrokinetic method as described in previous works.^{55,57–60} According to this approach, the electrophoretic mobility of PLL molecules in its dilute solutions (100–200 mg L⁻¹) is directly measured by applying the LDV technique. The results collected in Table 4 indicate that the mobility decreased with the NaCl concentration (ionic strength) from 4.5 $\mu\text{m cm (V s)}^{-1}$ (for 2×10^{-5} M ionic strength) to 2.1 $\mu\text{m cm (V s)}^{-1}$ (for 0.15 M ionic strength). This corresponds to the zeta potential of the molecule (calculated from the Henry model) of 82 and 40 mV. The positive value of the mobility confirms that the electrokinetic charge of PLL molecule remains positive for the above range of ionic strength and pH 5.4–5.6.

The diffusion coefficient of PLL molecules for various ionic strengths was determined by DLS as above described. It was equal to $1.5 \pm 0.4 \times 10^{-11} \text{ m}^2 \text{ s}^{-1}$ and $2.2 \pm 0.3 \times 10^{-11} \text{ m}^2 \text{ s}^{-1}$ at ionic strength of 2×10^{-5} and 0.15 M, respectively (see Table 4). It should be mentioned, however, that the precision of these measurements is limited for ionic strength below 10^{-3} M due to volume exclusion effects enhanced by the long-range electrostatic interactions among charged PLL molecules.

Knowing the electrophoretic mobility μ_e and the diffusion coefficient D , one can determine the electrokinetic (uncompensated) charge at PLL molecules from the previously used Lorentz–Stokes relationship:⁶¹

$$q = \frac{kT}{D} \mu_e \quad (3)$$

where k is the Boltzmann constant and T is the absolute temperature.

Consequently, the number of elementary charges N_e per one PLL molecule can be calculated from the formula:

$$N_c = q/e = 6.25 \times 10^{10} \frac{kT}{D} \mu_e \quad (4)$$

where D is expressed in $\text{m}^2 \text{s}^{-1}$, kT is expressed in J ($\text{kg m}^2 \text{s}^{-2}$) and μ_e is expressed in $\mu\text{m cm (V s)}^{-1}$.

It should be mentioned, that eq 3 is valid for an arbitrary charge distribution, the shape of molecules and for an arbitrary electrophoretic mobility. However, its accuracy decreases for larger ionic strengths where the double-layer thickness $\kappa^{-1} = (\epsilon kT/2e^2I)^{1/2}$ (where ϵ is the electric permittivity of the solvent, e is the elementary charge, $I = (\sum_i c_i z_i^2)/2$ is the ionic strength, c_i are the ion concentrations, z_i are the ion valences) becomes comparable with the PLL molecule diameter.

Using the experimental data obtained from electrophoresis (LDV) and DLS one obtains from eq 4 that N_c decreases with ionic strength from 75 (2×10^{-5} M) to 24 (0.15 M), see Table 4. Given that the number of monomers in the PLL molecule was equal to 584 this indicates that the electrokinetic charge is only a small fraction, ca. 4–13 % depending on ionic strength, of the nominal molecule charge. It is interesting to mention that such behavior was previously reported for PSS,⁶² PAH,⁶⁰ PDADMAC,⁵⁸ and for HSA molecules.⁶³

It should be mentioned that the electrokinetic charge is physically interpreted as that, which moves with the molecule, i.e., it is located below the shear plane.⁶⁴ Therefore, the electrokinetic charge is usually smaller (in absolute terms) than the condensed (specifically adsorbed) charge. This prediction is confirmed in the present case of PLL where the condensed charge predicted from MD modeling⁵⁶ was equal to 26% of the nominal charge of the molecule, which is ca. two times larger than the electrokinetic charge in the limit of low ionic strength.

Additionally, knowing the diffusion coefficient and the dynamic viscosity of the solution η one can calculate the hydrodynamic diameter d_H of the PLL molecule using the Stokes–Einstein relationship:

$$d_H = \frac{kT}{3\pi\eta D} \quad (5)$$

For ionic strength of 0.15 and 2×10^{-5} M one obtains from eq 5 $d_H = 22 \pm 3$ and 32 ± 8 nm, respectively (see Table 4). Because the hydrodynamic diameter is independent of the temperature and the solvent viscosity, it can be used for determining the PLL molecule dimensions.

Table 4. Experimental characteristics of PLL solutions at pH 5.4 – 5.6 and various NaCl concentrations.

I (M)	κ^{-1} (nm)	D ($\text{m}^2 \text{s}^{-1}$)	d_H (nm)	μ_e ($\mu\text{m cm (V s)}^{-1}$)	ζ (mV)	N_c	α^*
2×10^{-5}	68.7	$1.5 \pm 0.4 \times 10^{-11}$	32 ± 8	4.5 ± 0.25	82	75	0.13
10^{-4}	30.5	$1.6 \pm 0.4 \times 10^{-11}$	30 ± 7	4.2 ± 0.25	76	65	0.11
10^{-3}	9.63	$1.9 \pm 0.4 \times 10^{-11}$	26 ± 6	3.7 ± 0.25	70	50	0.085
10^{-2}	3.05	$2.0 \pm 0.3 \times 10^{-11}$	24 ± 4	3.5 ± 0.2	63	44	0.076
0.15	0.786	$2.2 \pm 0.3 \times 10^{-11}$	22 ± 3	2.1 ± 0.2	40	24	0.041

$\alpha^* = N_c/N_{mx}$ is the effective ionization degree

The above discussed results derived from MD modeling indicate that for lower ionic strength the PLL molecule shape can be approximated by a slender body characterized by the aspect ratio parameter λ much larger than unity. In this case, the hydrodynamic diameter can be expressed in the analytical form.^{65–67}

$$d_H = \frac{L_e}{(c_1 \ln 2\lambda + c_2)} = d_c \frac{\lambda}{c_1 \ln 2\lambda + c_2} = f_1(\lambda) \quad (6)$$

where c_1, c_2 are the dimensionless constants depending on the shape of the body.

For prolate spheroids $c_1 = 1, c_2 = 0$; for blunt cylinder $c_1 = 1, c_2 = -0.11$;^{68,69} for linear chain of touching beads $c_1 = 1, c_2 = -0.25$, for half circles $c_1 = 0.95, c_2 = 0.02$, and for a string of beads forming a torus $c_1 = 0.95, c_2 = 0.67$.^{68,69}

Taking the average value of $Le = 190$ nm and $\lambda = 206$ (see Table 3) one obtains from eq 6 32.1 nm (cylinder) and 32 nm (half circle). These values agree with experimental data obtained in the limit of low ionic strength within experimental error bounds.

One should remember, however, that the precision of hydrodynamic diameter determination becomes limited for the lower ionic strength range because of the uncertainty of the diffusion coefficient measurement induced by the electrostatic interactions among molecules in solution.

The aspect ratio parameter and the extended length of macroions can be more accurately determined via the dynamic viscosity measurement that was previously demonstrated in the case of PDADMAC solutions.⁵⁸

3.3. Dynamic Viscosity Measurements

Initially, the dependencies of the dynamic viscosity on PLL on its volume fraction $\Phi_V = c_b/\rho_p$ was measured (where c_b is the PLL mass concentration in the bulk) for various NaCl concentrations in the range of 2×10^{-5} to 0.15 M. The isotonic electrolyte solutions required for the lower ionic strength were prepared considering the above estimated PLL molecule ionization degree, which results in the following correction to the overall ionic strength:

$$I^* = \frac{1}{2} \times 10^{-6} N_c c_b / \overline{M}_n \quad (7)$$

where c_b is expressed in mg L^{-1} .

One can calculate from eq 7 that for $c_b = 50 \text{ mg L}^{-1}$ and N_c equal to 75, the ionic strength changes due to PLL dissociation amounts to ca. $2 \times 10^{-5} \text{ M}$.

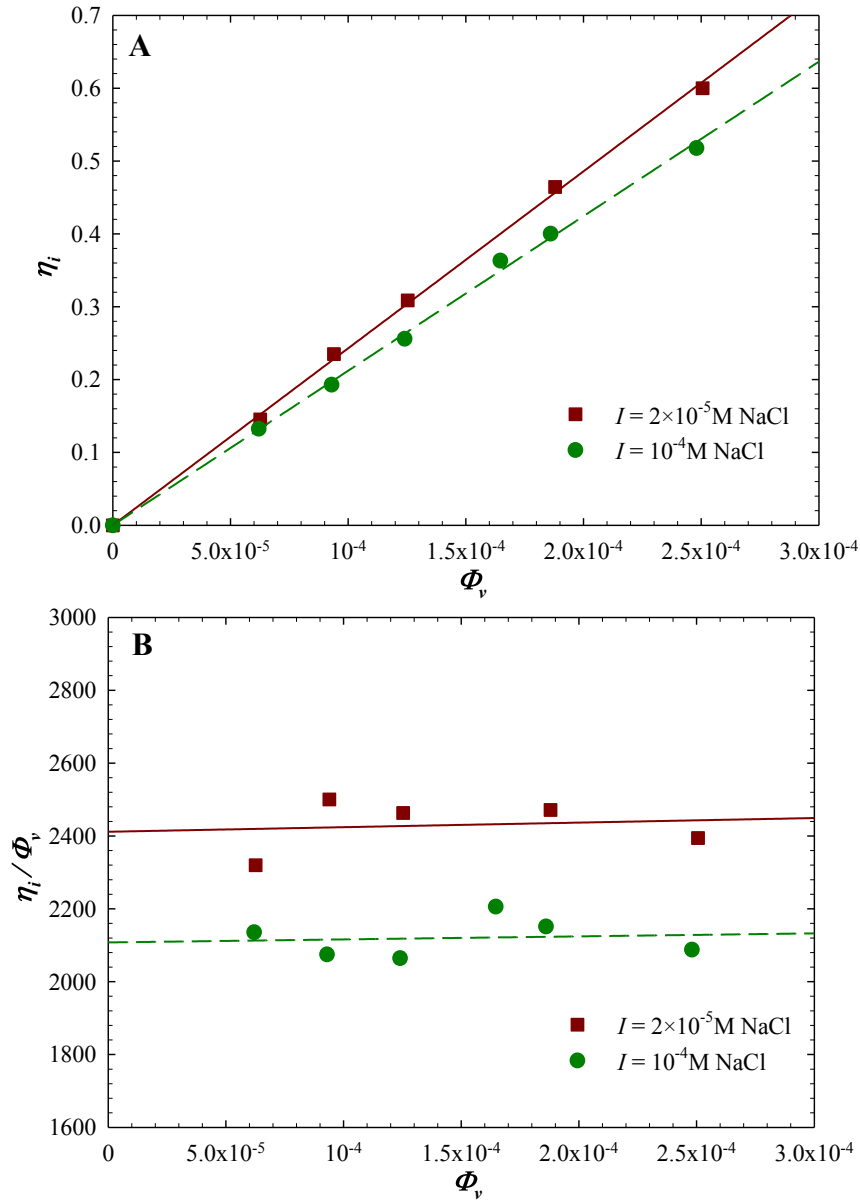


Figure 6. Part (A) The dependence of the relative viscosity increment η_i on the volume concentration of PLL solutions Φ_v . The solid line denotes a linear fit of experimental data. Part

(B) The dependence of η_i/Φ_V on the volume concentration of PLL solutions Φ_V . The solid lines denote the linear fits ($y = ax+b$) of experimental data.

The dependencies of the relative viscosity, η_i on the PLL volume fraction Φ_V acquired for $I = 2 \times 10^{-5}$ and 10^{-4} M is presented in Figure 6A. The slopes of these dependencies in the limit of low volume fractions, decreases from 2420 and 2110, respectively, corresponds to the intrinsic viscosity $[\eta]$ of PLL. The precision of this intrinsic viscosity determination can be increased by plotting η_i/Φ_V against Φ_V . The experimental results plotted in this way are shown in Figure 6B. The intrinsic viscosity is obtained as the intersection point of the line fitting the experimental data with the vertical axis. In this way one obtains $[\eta] = 2400$ and 2100 that agrees with the above value within experimental error bounds. The experimental values of the intrinsic viscosity obtained in this way for various ionic strengths are collected in Table 5.

One can observe that the increase in the intrinsic viscosity for ionic strength 2×10^{-5} M compared to 10^{-4} M amounts to only 15% although the double layer thickness increased more than two times. This confirms that the slender body regime is attained where the PLL molecules assume extended conformation theoretically predicted from MD modeling. Accordingly, as shown in previous works^{58,70} the intrinsic viscosity for the slender body regime can be calculated for $\lambda \gg 1$ from the formula:⁶⁸

$$[\eta] = c_{1v} \frac{\lambda^2}{\ln 2\lambda - 0.5} + c_{2v} \frac{\lambda^2}{\ln 2\lambda - 1.5} + c_v = f_v(\lambda) \quad (8)$$

where $c_{1v} = 3/15$, $c_{2v} = 1/15$ and c_v equals $14/15$ for blunt cylinders.

A numerical inversion of eq 8 yields the experimental value of the aspect ratio parameter:

$$\lambda = f_v^{-1}([\eta]) \quad (9)$$

However, because of relatively large dispersity index of PLL sample used in this work (see Table 3), one should first estimate the correction accounting for this effect. This becomes feasible if one considers that for an arbitrary molar mass distribution, the average value of a continuous function of macroion molar mass $f(M)$ can be calculated from the general formula (see Supporting Information section):

$$\bar{f} = f_0 \left[1 + C_f (\bar{M}_n) \bar{\sigma}_M^2 \right] \quad (10)$$

where $f_0 = f(\bar{M}_n)$, C_f is the dimensionless constant depending on \bar{M}_n , and $\bar{\sigma}_M$ is the normalized standard deviation of the molar mass distribution.

Considering eq 8 one can show that the correction to the experimentally measured intrinsic viscosity is explicitly given by (Supporting Information section):

$$[\eta_0] = [\eta] (1 + C_v \bar{\sigma}_M^2)^{-1} \quad (11)$$

where $[\eta_0]$ is the corrected intrinsic viscosity and the C_v constant is given by

$$C_v = 1 - \frac{3\beta_1^2 + 3\beta_2^2}{2\beta_1 + 3\beta_2} + \frac{\beta_1^3 + 3\beta_2^3}{\beta_1 + 3\beta_2} \quad (12)$$

where $\beta_1 = \frac{1}{\ln 2\lambda_0 - 0.5}$, $\beta_2 = \frac{1}{\ln 2\lambda_0 - 1.5}$, $\lambda_0 = \frac{L_e}{d_c}$.

Taking for example $\lambda_0 = 200$ one obtains $\beta_1 = 0.182$, $\beta_2 = 0.223$, and $C_v = 0.725$. Thus, for $\bar{\sigma}_M = 0.1$ (small macroion dispersity), $[\eta_0] = 0.993[\eta]$ and for $\bar{\sigma}_M = 0.3$ (large macroion dispersity), $[\eta_0] = 0.939[\eta]$. One can observe that the correction to intrinsic viscosity is relatively minor, ca. 6% even for large macroion dispersity.

In an analogous way, considering eq 6, the correction for the hydrodynamic diameter is described by:

$$d_{H_0} = d_H (1 + C_H \bar{\sigma}_M^{-2})^{-1} \quad (13)$$

where d_{H_0} is the corrected hydrodynamic diameter and the constant C_H is given by:

$$C_H = -c_1 \frac{0.5}{c_1 \ln 2\lambda_0 + c_2} + \frac{c_1^2}{c_1 (\ln 2\lambda_0 + c_2)^2} \quad (14)$$

Taking for example: $\lambda_0 = 200$, $c_1 = 1$, and $c_2 = -0.11$ (this corresponds to cylindrical shape of the molecule) one obtains $C_H = -0.056$. Thus, for $\bar{\sigma}_M = 0.3$, $d_{H_0} = 1.005 \bar{d}_H$. This indicates that the correction to the hydrodynamic diameter is practically negligible.

The dependence of the corrected intrinsic viscosity ionic strength and the double-layer thickness (upper horizontal axis) is plotted in Figure 7.

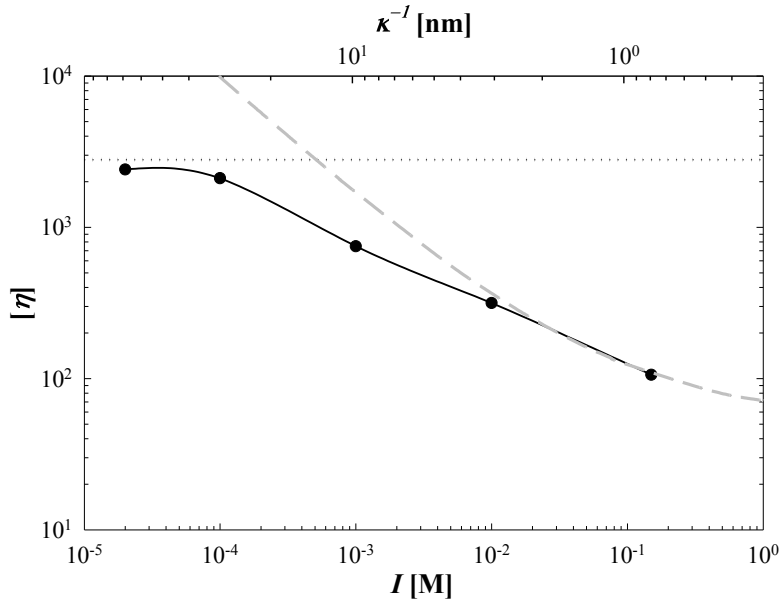


Figure 7. The dependence of the intrinsic viscosity $[\eta]$ of PLL molecules on the ionic strength I . The solid line denotes the non-linear fit of experimental data, the dotted line shows the theoretical slender body limit for a rod. The dashed line shows the theoretical results calculated from the interpolation formula of Rushing and Hester,⁷¹ i.e. $[\eta] = (14.1 + 11 \kappa^{-1.08})^{3/2}$.

One can observe that for ionic strength up to 10^{-2} M the experimental results are well reflected by the semi-empirical interpolation formula derived by Rushing and Hester.⁷¹ However, for lower ionic strength, the experimentally observed variation in the intrinsic viscosity become less abrupt that predicted by this formula because the molecules assume the most extended shape attaining the slender body limit (depicted by the dotted line in Figure 7).

The corrected values of the intrinsic viscosity are also collected in Table 5. Using the experimental data, one can calculate from eq 9 the λ_c parameter for the slender body cylinder model. Additionally, knowing λ_c and assuming that its volume is equal to molecule volume v_p (126 nm^3) one can calculate the effective length of the PLL molecule for various ionic strengths from the formula:

$$L_c = (4v_p \lambda_c^2 / \pi)^{1/3} \quad (15)$$

Table 5. Equivalent cylinder lengths and chain diameters for PLL molecules for various ionic strengths.

I (M)	$[\eta]$	$[\eta]^{\dagger}$	λ_c	L_c (nm)	d_c (nm)	S_g (nm ²)
0	-	2220	206*	190*	0.92*	175*
		2280**	209**	192**	0.92**	177**
2×10^{-5}	2420 ± 20	2270 ± 20	208	191	0.92	176
10^{-4}	2110 ± 20	1980 ± 20	194	182	0.94	171
10^{-3}	870 ± 20	820 ± 20	119	137	1.10 1.12**	145 153**
10^{-2}	320 ± 10	305 ± 10	68.0	91	1.33	118

0.15	120 ± 10	115 ± 10	43.0	66.6	1.55	100
------	----------	----------	------	------	------	-----

†Viscosity corrected for sample dispersity according to eq 11.

*Calculated from molar mass.

**Calculated from MD modeling for $N_m = 584$.

Consequently, the equivalent cylinder diameter can be calculated as $d_c = L_c/\lambda_c$. Values of λ_c , the effective length L_c , the diameter d_c , and the molecule cross-section area $S_g = d_c L_c$ calculated in this way are also given in Table 5. One can notice that the axis ratio parameter varies between 208 and 43 for ionic strength of 2×10^{-5} and 0.15 M, respectively. Since this length to width parameter remains much larger than unity, this validates the use of eq 8 for calculating the intrinsic viscosity in the case of cylinders.

It is interesting to mention that the equivalent cylinder lengths agree with the molecule end-to-end lengths theoretically predicted from the MD modelling for larger ionic strengths. Therefore, the results shown in Tables 5 indicate that even for the high ionic strength up to 0.15 M, PLL molecules assume an elongated shape characterized by the length to width ratio exceeding 43. These data have significance for interpreting PLL adsorption at various surfaces, which is often used for creating supporting layers for deposition,^{30,72–74} protein immobilization,^{11,75–78} and for producing macroion films in the layer-by-layer processes.^{79–82}

Another aspect of practical significance is that the intrinsic viscosity data can be used for the determination of the molar mass of macroions samples with a precision exceeding other conventional techniques. The basic steps of the method are as follows: initially the macroion intrinsic viscosity in the limit of low ionic strengths (preferably below 10^{-4} M) is determined applying dynamic viscosity measurements. In order to increase the precision of the intrinsic viscosity value one can apply a parabolic extrapolation of the experimental data to negligible

ionic strength. Then the aspect ratio parameter λ is calculated using the iterative scheme of inverting eq 8:

$$\lambda = \left(\frac{15 [\eta']}{f_1(\lambda_1)} \right)^{\frac{1}{2}} \quad (16)$$

where:

$$f_1(\lambda_1) = \frac{3}{(\ln 2\lambda_1 - 0.5)} + \frac{1}{(\ln 2\lambda_1 - 1.5)} \quad (17)$$

and $\lambda_1 = (15 [\eta'])^{\frac{1}{2}}$; $[\eta'] = [\eta] - c_v$. The precision of eq 16 is ca. 1% for the intrinsic viscosity range above 20.

Finally, considering that $\lambda d_c = Le = \frac{4\nu_p}{\pi d_c^2}$ and $\nu_p = 10^{-27} \frac{\bar{M}_n}{\rho_p A \nu}$ one can calculate the average

molar mass of macroion from the linear dependence:

$$\bar{M}_n = 10^{-27} \frac{\pi}{4} d_c^3 \rho_p A \nu \lambda = C_m \lambda \quad (18)$$

where:

$$C_m = 4.73 \times 10^{-4} d_c^3 \rho_p \quad (19)$$

One can observe that, in order to explicitly evaluation of eq 18 one needs the value of the macromolecule chain diameter. Hence for PLL, considering that $d_c = 0.92$ nm one obtains $C_m = 0.593$ kg mol⁻¹.

One can estimate using eq 11 that this simple scheme gives a 2% precision for the macroion samples characterized by $\bar{\sigma}_M < 0.2$. For macroion samples characterized by larger dispersity, for example 0.3, the precision is equal to 4%.

The utility of this method is illustrated by following examples. Taking the value of $[\eta] = 2420$ predicted for 2×10^{-5} M (see Table 5) one obtains from Eq. (16) $\lambda = 216$, hence $\overline{M}_n = 128$ kg mol⁻¹ (for $d_c = 0.92$ nm), which is only 5% above the experimental value derived by MALLS. For 10^{-4} M, taking $[\eta] = 2110$ one obtains from Eq. (16) $\lambda = 201$, hence $\overline{M}_n = 120$ kg mol⁻¹ (for $d_c = 0.92$ nm), which is only 2% below the experimental value derived by MALLS and electrophoresis.

It is also worth mentioning that it can be efficiently implemented without using internal molar mass standards.

4. Conclusions

Physicochemical properties of poly-L-lysine molecules were thoroughly determined by Molecular Dynamics (MD) modeling, DLS, LDV, and dynamic viscosity measurements.

The modeling enabled to calculate several parameters of primary significance that were not before known such as the density equal to 1.6×10^3 kg m⁻³, the chain diameter equal to 0.92 nm, and the monomer length was equal to 0.33 nm. The latter value allows to calculate the extended (contour) length of the molecule of arbitrary molar mass. Good agreement between experiments and theoretical results, indicates that the MD modeling can serve as a prediction tool of the polyelectrolyte properties in bulk solution. Additionally, the MD simulations provided detailed information about the polyelectrolyte conformation at molecular level, which helped with the experimental data interpretation.

These results enabled a quantitative interpretation of experimental data comprising the diffusion coefficient, the hydrodynamic diameter and intrinsic viscosity of molecules determined for the ionic strength range 2×10^{-5} to 0.15 M. Using the electrophoretic mobility and the

diffusion coefficient data it was determined that the electrokinetic charge of PLL molecules is considerably smaller than the nominal charge calculated from ionization equilibrium. Consequently, the effective ionization degree varied between 13 and 4 % for ionic strength of 2×10^{-5} and 0.15 M, respectively.

On the other hand, the dynamic viscosity measurements for dilute PLL solutions enabled to determine the intrinsic viscosity, which confirmed that PLL molecules assume extended conformations at all ionic strength. Thus, at ionic strength of 2×10^{-5} M the length of the molecule is equal to 190 nm, the chain diameter is equal to 0.92 nm and the cross-section area in the side-on orientation is equal to 176 nm^2 . At ionic strength of 10^{-3} M the experimentally determined length of the molecule is equal to 132 nm, the diameter 1.1 nm and the cross-section area in the side-on orientation is equal to 145 nm^2 .

These data enable to select optimum parameters for an efficient formation of PLL mono and multilayers on various substrates, which can serve as platforms for immobilization of nanoparticles and protein molecules. Also, the shell formation on microcapsules used in targeted drug delivery systems can be better controlled exploiting the above information about the PLL molecule conformations and charge under various physicochemical conditions.

Another aspect of practical significance is that the intrinsic viscosity data can be used for determination of the molar mass of PLL samples with a precision 1–4%, which exceeds the precision of other techniques. Information about the sample dispersity and internal standards are not required in order to efficiently implement this method.

ASSOCIATED CONTENT

Supporting Information

Determining corrections functions due to macroion dispersity (PDF).

AUTHOR INFORMATION

Corresponding Author

*E-mail: ncmorga@cyf-kr.edu.pl

ORCID

Maria Morga: 0000-0002-4913-9244

Dominik Kosior: 0000-0001-9549-4688

Piotr Batys: 0000-0002-2264-3053

Notes

The authors declare no competing financial interest.

ACKNOWLEDGMENTS

This work was financially supported by the National Science Centre Research Grant Sonata: UMO 2015/17/D/ST4/00569 (experimental measurements and quantitative analysis of viscosity studies); Opus Project UMO-2015/19/B/ST5/00847: (interpretation of the results). Piotr Batys gratefully acknowledges computational resources by the CSC IT Centre for Science, Finland (MD modeling).

REFERENCES

- (1) Bolto, B.; Gregory, J. Organic Polyelectrolytes in Water Treatment. *Water Res.* **2007**, *41* (11), 2301–2324.

- (2) Nicu, R.; Bobu, E.; Desbrieres, J. Chitosan as Cationic Polyelectrolyte in Wet-End Papermaking Systems. *Cellul. Chem. Technol.* **2011**, *45* (1), 105–111.
- (3) Zhu, X.; Jańczewski, D.; Lee, S. S. C.; Teo, S. L.-M.; Vancso, G. J. Cross-Linked Polyelectrolyte Multilayers for Marine Antifouling Applications. *ACS Appl. Mater. Interfaces* **2013**, *5* (13), 5961–5968.
- (4) Wang, S.; Chen, K.; Xu, Y.; Yu, X.; Wang, W.; Li, L.; Guo, X. Protein Immobilization and Separation Using Anionic/Cationic Spherical Polyelectrolyte Brushes Based on Charge Anisotropy. *Soft Matter* **2013**, *9* (47), 11276–11287.
- (5) Wang, D.; Gong, X.; Heeger, P. S.; Rininsland, F.; Bazan, G. C.; Heeger, A. J. Biosensors from Conjugated Polyelectrolyte Complexes. *Proc. Natl. Acad. Sci.* **2002**, *99* (1), 49–53.
- (6) Luo, R.; Venkatraman, S. S.; Neu, B. Layer-by-Layer Polyelectrolyte–Polyester Hybrid Microcapsules for Encapsulation and Delivery of Hydrophobic Drugs. *Biomacromolecules* **2013**, *14* (7), 2262–2271.
- (7) Ariga, K.; Lvov, Y. M.; Kawakami, K.; Ji, Q.; Hill, J. P. Layer-by-Layer Self-Assembled Shells for Drug Delivery. *Adv. Drug Deliv. Rev.* **2011**, *63* (9), 762–771.
- (8) Wang, Y.; Chang, Y. C. Synthesis and Conformational Transition of Surface-Tethered Polypeptide: Poly(L-Lysine). *Macromolecules* **2003**, *36* (17), 6511–6518.
- (9) Dos, A.; Schimming, V.; Tosoni, S.; Limbach, H.-H. Acid–Base Interactions and Secondary Structures of Poly-L-Lysine Probed by ¹⁵N and ¹³C Solid State NMR and Ab Initio Model Calculations. *J. Phys. Chem. B* **2008**, *112* (49), 15604–15615.

- (10) Kaminskas, L. M.; Kelly, B. D.; McLeod, V. M.; Boyd, B. J.; Krippner, G. Y.; Williams, E. D.; Porter, C. J. H. Pharmacokinetics and Tumor Disposition of PEGylated, Methotrexate Conjugated Poly-L-Lysine Dendrimers. *Mol. Pharm.* **2009**, *6* (4), 1190–1204.
- (11) Patel, L. N.; Zaro, J. L.; Shen, W.-C. Cell Penetrating Peptides: Intracellular Pathways and Pharmaceutical Perspectives. *Pharm. Res.* **2007**, *24* (11), 1977–1992.
- (12) Deming, T. J. Methodologies for Preparation of Synthetic Block Copolypeptides: Materials with Future Promise in Drug Delivery. *Adv. Drug Deliv. Rev.* **2002**, *54* (8), 1145–1155.
- (13) de Vos, P.; van Hoogmoed, C. G.; van Zanten, J.; Netter, S.; Strubbe, J. H.; Busscher, H. J. Long-Term Biocompatibility, Chemistry, and Function of Microencapsulated Pancreatic Islets. *Biomaterials* **2003**, *24* (2), 305–312.
- (14) Clayton, H. A.; James, R. F. L.; London, N. J. M. Islet Microencapsulation: A Review. *Acta Diabetol.* **1993**, *30* (4), 181–189.
- (15) Murua, A.; Portero, A.; Orive, G.; Hernández, R. M.; de Castro, M.; Pedraz, J. L. Cell Microencapsulation Technology: Towards Clinical Application. *J. Controlled Release* **2008**, *132* (2), 76–83.
- (16) Lim, F.; Moss, R. D. Microencapsulation of Living Cells and Tissues. *J. Pharm. Sci.* **1981**, *70* (4), 351–354.
- (17) Haque, T.; Chen, H.; Ouyang, W.; Martoni, C.; Lawuyi, B.; Urbanska, A. M.; Prakash, S. Superior Cell Delivery Features of Poly(ethylene Glycol) Incorporated Alginate, Chitosan, and Poly-L-Lysine Microcapsules. *Mol. Pharm.* **2005**, *2* (1), 29–36.

- (18) Rajendra, B. R.; Sciorra, L. J.; Lee, M. A New and Simple Technique for Chromosomal Preparations from Peripheral Blood Lymphocytes, Amniotic Cell Cultures, Skin Fibroblasts, Bone Marrow and Single Cell Clones When the Yields from Harvests Are Low. *Hum. Genet.* **1980**, *55* (3), 363–366.
- (19) Bolduc, O. R.; Clouthier, C. M.; Pelletier, J. N.; Masson, J.-F. Peptide Self-Assembled Monolayers for Label-Free and Unamplified Surface Plasmon Resonance Biosensing in Crude Cell Lysate. *Anal. Chem.* **2009**, *81* (16), 6779–6788.
- (20) Statz, A. R.; Meagher, R. J.; Barron, A. E.; Messersmith, P. B. New Peptidomimetic Polymers for Antifouling Surfaces. *J. Am. Chem. Soc.* **2005**, *127* (22), 7972–7973.
- (21) Goodman, S. B.; Yao, Z.; Keeney, M.; Yang, F. The Future of Biologic Coatings for Orthopaedic Implants. *Biomaterials* **2013**, *34* (13), 3174–3183.
- (22) Kranz, B. R.; Thiel, E.; Thierfelder, S. Immunocytochemical Identification of Meningeal Leukemia and Lymphoma: Poly-L-Lysine-Coated Slides Permit Multimarker Analysis Even with Minute Cerebrospinal Fluid Cell Specimens. *Blood* **1989**, *73* (7), 1942–1950.
- (23) Myer, Y. P. The pH-Induced Helix-Coil Transition of Poly-L-Lysine and Poly-L-Glutamic Acid and the 238-M μ Dichroic Band. *Macromolecules* **1969**, *2* (6), 624–628.
- (24) Satake, I.; Yang, J. T. Effect of Temperature and pH on the B-helix Transition of poly(L-Lysine) in Sodium Dodecyl Sulfate Solution. *Biopolymers* **1975**, *14* (9), 1841–1846.
- (25) Shepherd, I. W. Study of Poly-L-Lysine Conformations in Aqueous Methanol Solution by Using Polarized Raman Techniques. *Biochem. J.* **1976**, *155* (3), 543–548.

- (26) Picart, C.; Lavalle, P.; Hubert, P.; Cuisinier, F. J. G.; Decher, G.; Schaaf, P.; Voegel, J.-C. Buildup Mechanism for Poly(L-Lysine)/Hyaluronic Acid Films onto a Solid Surface. *Langmuir* **2001**, *17* (23), 7414–7424.
- (27) Verma, A.; Stellacci, F. Effect of Surface Properties on Nanoparticle–Cell Interactions. *Small* **2010**, *6* (1), 12–21.
- (28) Frey, B. L.; Jordan, C. E.; Kornguth, S.; Corn, R. M. Control of the Specific Adsorption of Proteins onto Gold Surfaces with Poly (L-Lysine) Monolayers. *Anal. Chem.* **1995**, *67* (24), 4452–4457.
- (29) Richert, L.; Arntz, Y.; Schaaf, P.; Voegel, J.-C.; Picart, C. pH Dependent Growth of poly(L-Lysine)/poly(L-Glutamic) Acid Multilayer Films and Their Cell Adhesion Properties. *Surf. Sci.* **2004**, *570* (1–2), 13–29.
- (30) Hartono, S. B.; Gu, W.; Kleitz, F.; Liu, J.; He, L.; Middelberg, A. P. J.; Yu, C.; Lu, G. Q. (Max); Qiao, S. Z. Poly-L-Lysine Functionalized Large Pore Cubic Mesostructured Silica Nanoparticles as Biocompatible Carriers for Gene Delivery. *ACS Nano* **2012**, *6* (3), 2104–2117.
- (31) Barrantes, A.; Santos, O.; Sotres, J.; Arnebrant, T. Influence of pH on the Build-up of Poly-L-Lysine/Heparin Multilayers. *J. Colloid Interface Sci.* **2012**, *388* (1), 191–200.
- (32) Barrantes, A.; Wengenroth, J.; Arnebrant, T.; Haugen, H. J. Poly-L-Lysine/Heparin Multilayer Coatings Prevent Blood Protein Adsorption. *J. Colloid Interface Sci.* **2017**, *485*, 288–295.

(33) Porus, M.; Maroni, P.; Borkovec, M. Structure of Adsorbed Polyelectrolyte Monolayers Investigated by Combining Optical Reflectometry and Piezoelectric Techniques. *Langmuir* **2012**, *28* (13), 5642–5651.

(34) Porus, M.; Maroni, P.; Borkovec, M. Response of Adsorbed Polyelectrolyte Monolayers to Changes in Solution Composition. *Langmuir* **2012**, *28* (50), 17506–17516.

(35) Choi, J.-H.; Kim, S.-O.; Linardy, E.; Dreaden, E. C.; Zhdanov, V. P.; Hammond, P. T.; Cho, N.-J. Influence of pH and Surface Chemistry on Poly(L-Lysine) Adsorption onto Solid Supports Investigated by Quartz Crystal Microbalance with Dissipation Monitoring. *J. Phys. Chem. B* **2015**, *119* (33), 10554–10565.

(36) Craig, M.; Holmberg, K.; Le Ru, E.; Etchegoin, P. Polypeptide Multilayer Self-Assembly Studied by Ellipsometry. *J. Drug Deliv.* **2014**, *2014*, 1–5.

(37) Craig, M.; Bordes, R.; Holmberg, K. Polypeptide Multilayer Self-Assembly and Enzymatic Degradation on Tailored Gold Surfaces Studied by QCM-D. *Soft Matter* **2012**, *8* (17), 4788–4794.

(38) Ren, K.; Ji, J.; Shen, J. Construction and Enzymatic Degradation of Multilayered Poly-L-Lysine/DNA Films. *Biomaterials* **2006**, *27* (7), 1152–1159.

(39) Shan, C.; Yang, H.; Han, D.; Zhang, Q.; Ivaska, A.; Niu, L. Water-Soluble Graphene Covalently Functionalized by Biocompatible Poly-L-Lysine. *Langmuir* **2009**, *25* (20), 12030–12033.

- (40) Morga, M.; Adamczyk, Z.; Gödrich, S.; Oćwieja, M.; Papastavrou, G. Monolayers of Poly-L-Lysine on Mica – Electrokinetic Characteristics. *J. Colloid Interface Sci.* **2015**, *456*, 116–124.
- (41) Morga, M.; Michna, A.; Adamczyk, Z. Formation and Stability of Polyelectrolyte/Polypeptide Monolayers Determined by Electrokinetic Measurements. *Colloids Surf. Physicochem. Eng. Asp.* **2017**, *529*, 302–310.
- (42) Berendsen, H. J. C.; van der Spoel, D.; van Drunen, R. Gromacs: A Message-Passing Parallel Molecular Dynamics Implementation. *Comput. Phys. Commun.* **1995**, *91* (1), 43–56.
- (43) Lindahl, E.; Hess, B.; van der. Spoel, D. Gromacs 3.0: A Package for Molecular Simulation and Trajectory Analysis. *Mol. Model. Annu.* **2001**, *7* (8), 306–317.
- (44) Duan, Y.; Wu, C.; Chowdhury, S.; Lee, M. C.; Xiong, G.; Zhang, W.; Yang, R.; Cieplak, P.; Luo, R.; Lee, T.; et al. A Point-Charge Force Field for Molecular Mechanics Simulations of Proteins Based on Condensed-Phase Quantum Mechanical Calculations. *J. Comput. Chem.* **2003**, *24* (16), 1999–2012.
- (45) Jorgensen, W. L.; Chandrasekhar, J.; Madura, J. D.; Impey, R. W.; Klein, M. L. Comparison of Simple Potential Functions for Simulating Liquid Water. *J. Chem. Phys.* **1983**, *79* (2), 926–935.
- (46) Hanwell, M. D.; Curtis, D. E.; Lonie, D. C.; Vandermeersch, T.; Zurek, E.; Hutchison, G. R. Avogadro: An Advanced Semantic Chemical Editor, Visualization, and Analysis Platform. *J. Cheminformatics* **2012**, *4*, 1–17.

- (47) Bussi, G.; Donadio, D.; Parrinello, M. Canonical Sampling through Velocity Rescaling. *J. Chem. Phys.* **2007**, *126* (1), 1–7.
- (48) Parrinello, M.; Rahman, A. Polymorphic Transitions in Single Crystals: A New Molecular Dynamics Method. *J. Appl. Phys.* **1981**, *52* (12), 7182–7190.
- (49) Essmann, U.; Perera, L.; Berkowitz, M. L.; Darden, T.; Lee, H.; Pedersen, L. G. A Smooth Particle Mesh Ewald Method. *J. Chem. Phys.* **1995**, *103* (19), 8577–8593.
- (50) Hess, B.; Bekker, H.; Berendsen, H. J. C.; Fraaije, J. G. E. M. LINCS: A Linear Constraint Solver for Molecular Simulations. *J Comput Chem* **1997**, 1463–1472.
- (51) Miyamoto, S.; Kollman, P. A. Settle: An Analytical Version of the Shake and Rattle Algorithm for Rigid Water Models. *J. Comput. Chem.* **1992**, *13* (8), 952–962.
- (52) Humphrey, W.; Dalke, A.; Schulten, K. VMD: Visual Molecular Dynamics. *J. Mol. Graph.* **1996**, *14* (1), 33–38.
- (53) Kuhn, H.; Kuhn, W. Effects of Hampered Draining of Solvent on the Translatory and Rotatory Motion of Statistically Coiled Long-Chain Molecules in Solution. Part I. Translation Resistance; Rate of Diffusion and Sedimentation. *J. Polym. Sci.* **1950**, *5* (5), 519–541.
- (54) Inoue, T.; Osaki, K. Role of Polymer Chain Flexibility on the Viscoelasticity of Amorphous Polymers around the Glass Transition Zone. *Macromolecules* **1996**, *29* (5), 1595–1599.
- (55) Michna, A.; Adamczyk, Z.; Kubiak, K.; Jamróży, K. Formation of PDADMAC Monolayers Evaluated in Situ by QCM and Streaming Potential Measurements. *J. Colloid Interface Sci.* **2014**, *428*, 170–177.

- (56) Batys, P.; Luukkonen, S.; Sammalkorpi, M. Ability of the Poisson–Boltzmann Equation to Capture Molecular Dynamics Predicted Ion Distribution around Polyelectrolytes. *Phys. Chem. Chem. Phys.* **2017**, *19* (36), 24583–24593.
- (57) Adamczyk, Z.; Michna, A.; Szaraniec, M.; Bratek, A.; Barbasz, J. Characterization of Poly(ethylene Imine) Layers on Mica by the Streaming Potential and Particle Deposition Methods. *J. Colloid Interface Sci.* **2007**, *313* (1), 86–96.
- (58) Adamczyk, Z.; Jamróży, K.; Batys, P.; Michna, A. Influence of Ionic Strength on Poly(diallyldimethylammonium Chloride) Macromolecule Conformations in Electrolyte Solutions. *J. Colloid Interface Sci.* **2014**, *435* (Supplement C), 182–190.
- (59) Michna, A.; Adamczyk, Z.; Batys, P. Mapping Single Macromolecule Chains Using the Colloid Deposition Method: PDADMAC on Mica. *J. Colloid Interface Sci.* **2015**, *450*, 82–90.
- (60) Adamczyk, Z.; Zembala, M.; Michna, A. Polyelectrolyte Adsorption Layers Studied by Streaming Potential and Particle Deposition. *J. Colloid Interface Sci.* **2006**, *303* (2), 353–364.
- (61) Adamczyk, Z.; Zembala, M.; Warszyński, P.; Jachimska, B. Characterization of Polyelectrolyte Multilayers by the Streaming Potential Method. *Langmuir* **2004**, *20* (24), 10517–10525.
- (62) Adamczyk, Z.; Jachimska, B.; Jasiński, T.; Warszyński, P.; Wasilewska, M. Structure of Poly (Sodium 4-Styrenesulfonate) (PSS) in Electrolyte Solutions: Theoretical Modeling and Measurements. *Colloids Surf. Physicochem. Eng. Asp.* **2009**, *343* (1), 96–103.

- (63) Dąbkowska, M.; Adamczyk, Z. Ionic Strength Effect in HSA Adsorption on Mica Determined by Streaming Potential Measurements. *J. Colloid Interface Sci.* **2012**, *366* (1), 105–113.
- (64) Hunter, R. J. *Zeta Potential in Colloid Science: Principles and Applications*; Colloid science; Academic Press: London, 1981.
- (65) Davis, R. M.; Russel, W. B. On the Theory of Dilute Polyelectrolyte Solutions: Extensions, Refinements, and Experimental Tests. *J. Polym. Sci. Part B Polym. Phys.* **1986**, *24* (3), 511–533.
- (66) Adamczyk, Z.; Cichocki, B.; Ekiel-Jeżewska, M. L.; Słowicka, A.; Wajnryb, E.; Wasilewska, M. Fibrinogen Conformations and Charge in Electrolyte Solutions Derived from DLS and Dynamic Viscosity Measurements. *J. Colloid Interface Sci.* **2012**, *385* (1), 244–257.
- (67) Mansfield, M. L.; Douglas, J. F. Transport Properties of Rodlike Particles. *Macromolecules* **2008**, *41* (14), 5422–5432.
- (68) Brenner, H. Rheology of a Dilute Suspension of Axisymmetric Brownian Particles. *Int. J. Multiph. Flow* **1974**, *1* (2), 195–341.
- (69) Adamczyk, Z.; Bratek, A.; Jachimska, B.; Jasiński, T.; Warszyński, P. Structure of Poly(acrylic Acid) in Electrolyte Solutions Determined from Simulations and Viscosity Measurements. *J. Phys. Chem. B* **2006**, *110* (45), 22426–22435.
- (70) Jachimska, B.; Jasiński, T.; Warszyński, P.; Adamczyk, Z. Conformations of Poly(allylamine Hydrochloride) in Electrolyte Solutions: Experimental Measurements and Theoretical Modeling. *Colloids Surf. Physicochem. Eng. Asp.* **2010**, *355* (1–3), 7–15.

(71) Rushing, T. S.; Hester, R. D. Semi-Empirical Model for Polyelectrolyte Intrinsic Viscosity as a Function of Solution Ionic Strength and Polymer Molecular Weight. *Polymer* **2004**, *45* (19), 6587–6594.

(72) Farkas, E.; Srankó, D.; Kerner, Z.; Setner, B.; Szewczuk, Z.; Malinka, W.; Horvath, R.; Szyrwił, Ł.; Pap, J. S. Self-Assembled, Nanostructured Coatings for Water Oxidation by Alternating Deposition of Cu-Branched Peptide Electrocatalysts and Polyelectrolytes. *Chem Sci* **2016**, *7* (8), 5249–5259.

(73) Jiang, X.; Tong, M.; Li, H.; Yang, K. Deposition Kinetics of Zinc Oxide Nanoparticles on Natural Organic Matter Coated Silica Surfaces. *J. Colloid Interface Sci.* **2010**, *350* (2), 427–434.

(74) Zhao, L.; Zhao, L.; Yang, S.; Peng, X.; Wu, J.; Bian, L.; Wang, X.; Pu, Q. Use of Pulsed Streaming Potential with a Prepared Cationic Polyelectrolyte Layer to Detect Deposition Kinetics of Graphene Oxide and Consequences of Particle Size Differences. *Anal. Chem.* **2016**, *88* (21), 10437–10444.

(75) Silva, J. M.; García, J. R.; Reis, R. L.; García, A. J.; Mano, J. F. Tuning Cell Adhesive Properties via Layer-by-Layer Assembly of Chitosan and Alginate. *Acta Biomater.* **2017**, *51*, 279–293.

(76) Wei, Q.; Becherer, T.; Angioletti-Uberti, S.; Dzubiella, J.; Wischke, C.; Neffe, A. T.; Lendlein, A.; Ballauff, M.; Haag, R. Protein Interactions with Polymer Coatings and Biomaterials. *Angew. Chem. Int. Ed.* **2014**, *53* (31), 8004–8031.

(77) Mann, A.; Richa, R.; Ganguli, M. DNA Condensation by Poly-L-Lysine at the Single Molecule Level: Role of DNA Concentration and Polymer Length. *J. Controlled Release* **2008**, *125* (3), 252–262.

(78) Yamagata, M.; Kawano, T.; Shiba, K.; Mori, T.; Katayama, Y.; Niidome, T. Structural Advantage of Dendritic Poly(l-Lysine) for Gene Delivery into Cells. *Bioorg. Med. Chem.* **2007**, *15* (1), 526–532.

(79) Borges, J.; Mano, J. F. Molecular Interactions Driving the Layer-by-Layer Assembly of Multilayers. *Chem. Rev.* **2014**, *114* (18), 8883–8942.

(80) Westwood, M.; Noel, T. R.; Parker, R. The Effect of Poly-L-Lysine Structure on the pH Response of Polygalacturonic Acid-Based Multilayers. *Carbohydr. Polym.* **2013**, *94* (1), 137–146.

(81) Tang, Z.; Wang, Y.; Podsiadlo, P.; Kotov, N. A. Biomedical Applications of Layer-by-Layer Assembly: From Biomimetics to Tissue Engineering. *Adv. Mater.* **2006**, *18* (24), 3203–3224.

(82) Orive, G.; Tam, S.; Pedraz, J.; Halle, J. Biocompatibility of Alginate-poly-L-Lysine Microcapsules for Cell Therapy? *Biomaterials* **2006**, *27* (20), 3691–3700.

TOC Graphic

